Journal of Harbin Engineering University
ISSN: 1006-7043

Vol 47 No. 08
Aug 2026

Dynamic Intereaction Analysis between Hybrid Suspension and Burckhardt Tire Characterization on Lateral Stability Limit a 1.25-Ton Commercial Truck

Khoi Phan Chuong Anh[1] Tung Nguyen Thanh[1] Vu Duong[2*]

[1] Vinh Long University of Technology Education, 73 Nguyen Hue, Long Chau, Vinh Long Vietnam
[2]School of Engineering and Technology, Duy Tan University, 03 Quang Trung, Hai Chau, Da Nang, Viet Nam

Abstract: This study investigates the lateral stability limits of a 1.25-ton commercial truck equipped with a hybrid suspension system, in which the front axle uses a mechanical suspension and the rear axle uses a pneumatic suspension. A spatial multibody dynamic model is combined with the Burckhardt tire model to describe road-dependent tire friction characteristics. The vehicle is simulated under a J-turn maneuver to examine the effects of vehicle speed, road adhesion, and axle-dependent load transfer on rollover and side-slip tendencies. The stability response is evaluated using lateral acceleration, roll angle, load transfer ratio LTR, and maximum combined tire friction utilization. The results show that, on dry asphalt, vehicle speed strongly increases rollover risk: the truck remains stable at 30 km/h, reaches a rollover warning state at 40 km/h with LTRmax = 0.922, and experiences wheel lift-off from 50 km/h. At 60 km/h, rollover and tire friction saturation occur simultaneously. On wet gravel and ice, LTR remains below the rollover warning threshold, while tire friction utilization reaches unity, indicating side-slip dominance. The hybrid suspension also causes uneven axle load transfer, with higher LTR at the front axle. The findings provide a basis for defining rollover-side-slip warning thresholds.

1 Introduction

Light commercial trucks are widely used in freight transport due to their load-carrying capacity and high flexibility. However, when operating under fully loaded conditions, negotiating curves, or executing sudden steering maneuvers, their lateral stability can significantly deteriorate. This is primarily attributed to an increased center of gravity (CG) height, altered load distribution, and a limited track width. Accident statistics and previous studies indicate that lateral instability is a major cause of severe truck accidents, particularly during high-speed cornering or emergency evasive maneuvers [1,3].The lateral instability of vehicles is generally classified into two primary mechanisms: directional instability side-slip and rollover[4-6].Directional instability typically occurs on low-friction road surfaces when the tire-road adhesion limit is saturated. Conversely, rollover tends to happen on high-friction surfaces [i] where the tires can still generate substantial lateral forces, but a severe vertical load transfer occurs from the inner to the outer wheels. Consequently, determining the lateral stability limits of a truck requires a simultaneous evaluation of the vehicle body motion, dynamic load transfer through the suspension system, and tire-road interaction characteristics.In lateral stability research, the multibody system approach combined with Newton-Euler equations is widely utilized to describe the spatial dynamics of heavy trucks, multi-axle vehicles, and tractor-semitrailers [7,8]. The Load Transfer Ratio (LTR) is commonly used as an index to evaluate the risk of wheel lift-off and rollover. As the LTR approaches 1, the vertical load on the inner wheels nears zero, indicating a critical rollover condition[9]. Additionally, lateral acceleration, yaw rate, roll angle, and sideslip angle are essential parameters for describing the vehicle's stability response during steering maneuvers [10,11]. Regarding tire-road interaction, the Burckhardt tire model is highly suitable for capturing the variations in friction forces under different slip states and road conditions, particularly as the vehicle approaches its stability limits [12,13,14].Although several studies have addressed rollover and side slip of heavy trucks, multi-axle vehicles, and articulated combinations, the lateral stability boundary of light commercial trucks equipped with hybrid suspension systems has not been sufficiently clarified. The reasons for the insufficient study consist of variable center of gravity, elastokinematic complexity, and the definition of the stability boundary. In such vehicles, the front mechanical suspension and the rear pneumatic suspension may generate different roll stiffness and load transfer characteristics. This asymmetry can affect not only the rollover tendency but also the tire friction saturation process under different road adhesion conditions. Motivated by this research gap, this study clarifies how the hybrid suspension structure interacts with Burckhardt tire characteristics in determining the transition boundary between rollover and side-slip instability for a 1.25-ton commercial truck.

2 Dynamic Model and Evaluation Criteria

2.1 Vehicle Model Description

The investigated vehicle is a 1.25-ton, two-axle commercial truck equipped with a hybrid suspension system.Specifically, the front axle features a mechanical suspension, while the rear axle employs an air suspension system. The model is developed based on the multibody system approach, consisting of three primary rigid bodies: the sprung mass of the vehicle body m_C, the front unsprung mass m_{A1}, and the rear unsprung mass m_{A2}.

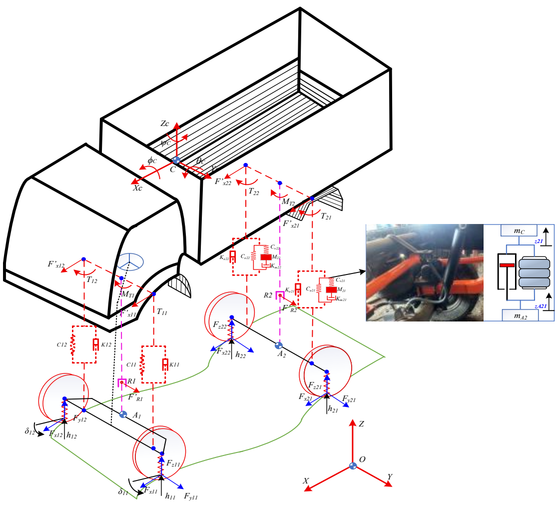

Figure.1. Schematic diagram of the dynamic model of a truck using

a hybrid suspension system.

The vehicle body is modeled with six degrees of freedom (6-DOF) within a body-fixed coordinate system. This includes three translational motions along the longitudinal, lateral, and vertical axes, alongside three rotational motions, ϕ_C, θ_C, ψ_C namely roll, pitch, and yaw. J_{xC}, J_{yC}, J_{zC} .To represent the spatial dynamics and the moments of inertia of the vehicle body, the generalized coordinate vector of the sprung mass is defined as follows:

Equation of translation force:

$$m_C(\ddot{x}_C - \dot{y}_C\dot{\psi}_C + \dot{z}_C\dot{\theta}_C) = FX$$
$$m_C(\ddot{y}_C - \dot{z}_C\dot{\phi}_C + \dot{x}_C\dot{\psi}_C) = FY$$
$$m_C(\ddot{z}_C - \dot{x}_C\dot{\theta}_C + \dot{y}_C\dot{\phi}_C) = FZ$$

Moment of rotation equation: (2.1)

$$J_{xC}\ddot{\phi}_C + (J_{zC} - J_{yC})\dot{\psi}_C\dot{\theta}_C = MX$$
$$J_{yC}\ddot{\theta}_C + (J_{xC} - J_{zC})\dot{\phi}_C\dot{\psi}_C = MY$$
$$J_{zC}\ddot{\psi}_C + (J_{yC} - J_{xC})\dot{\theta}_C\dot{\phi}_C = MZ$$

Here, x, y, and z denote the translational displacements of the sprung mass center of gravity, while ϕ_C, θ_C, and ψ_C represent the roll, pitch, and yaw angles of the vehicle body, respectively.

The primary assumptions of the mathematical model are as follows:

- The vehicle is structurally symmetric about its longitudinal center plane.
- The compliance of the steering system is neglected.
- The road surface is assumed to be perfectly flat during the J-turn maneuver.
- Tire-road interaction forces are determined using the Burckhardt tire model.
- The effects of aerodynamic crosswinds are not considered within the scope of this study.

The dynamic equations of motion for the truck's sprung mass are formulated as follows:

$$FX = F'_{x11} + F'_{x12} + F'_{x21} + F'_{x22} + m_C g \sin\theta_C - F_{wx}$$

$$FY = F_{R1}^{'} + F_{R2}^{'} - m_C g \cos\theta_C \sin\phi_C + F_{wy}$$

$$FZ = (F_{CK11} + F_{CK12}) + (F_{AirK21} + F_{AirK22}) + m_C g(1 - \cos\theta_C \cos\phi_C)$$

$$MX = w_1(F_{CK11} - F_{CK12}) + w_2(F_{AirK21} - F_{AirK22}) + (h_{CG} - h_{R1})F_{R1}^{'} \\ +(h_{CG} - h_{R2})F_{R2}^{'} - (h_w - h_{CG})F_{wy} - (M_{T1} + M_{T2})$$

$$MY = -l_1(F_{CK11} + F_{CK12}) + l_2(F_{AirK21} + F_{AirK22}) - (h_w - h_{CG})F_{wx} \\ -(h_{CG} - r_{t1})(F_{x11}^{'} + F_{x12}^{'}) - (h_{CG} - r_{t2})(F_{x21}^{'} + F_{x22}^{'}) - (T_{11} + T_{12} + T_{21} + T_{22})$$

$$MZ = w_1(F_{x12}^{'} - F_{x11}^{'}) + w_2(F_{x22}^{'} - F_{x21}^{'}) + l_1 F_{R1}^{'} - l_2 F_{R2}^{'} + F_{wy} h_w$$

(2.2)

Where: Along the longitudinal axis, the total force consists of the longitudinal forces transmitted from both axles to the chassis, the aerodynamic drag, and the dynamic weight component induced by the pitch angle. Along the lateral axis, the total force includes the lateral reaction forces at the roll centers of the front and rear axles, the aerodynamic crosswind force, and the lateral weight component caused by the roll angle. Along the vertical axis, a distinct feature of this hybrid model is that the total vertical force is composed of the elastic and damping forces from the front mechanical suspension, combined with the nonlinear pneumatic lifting force derived from the GENSYS model and the rear damping forces.The equations of motion for the unsuspended masses of the vehicle axles are written as follows:

$$m_{A1}\ddot{z}_{A1} - m_{A1}(\dot{x}_{A1}\dot{\theta}_{A1} - \dot{y}_{A1}\dot{\phi}_{A1}) = (F_{CL11} + F_{CL12}) - (F_{CK11} + F_{CK12}) + m_{A1}g(1 - \cos\theta_{A1}\sin\phi_{A1})$$

$$m_{A1}\ddot{y}_{A1} - m_{A1}(\dot{z}_{A1}\dot{\phi}_{A1} - \dot{x}_{A1}\dot{\psi}_{A1}) = F_{x11}\sin\delta_{11} + F_{x12}\sin\delta_{12} + F_{y11}\cos\delta_{11} \\ +F_{y12}\cos\delta_{12} - F_{R1} - m_{A1}g\cos\theta_{A1}\sin\phi_{A1}$$

$$J_{xA1}\ddot{\phi}_{A1} - (J_{yA1} - J_{zA1})\dot{\psi}_{A1}\dot{\theta}_{A1} = (F_{CL11} - F_{CL12})b_1 + (F_{CK12} - F_{CK11})w_1 + F_{R1}(h_{R1} - r_{t1}) \\ +(F_{x11}\sin\delta_{11} + F_{x12}\sin\delta_{12} + F_{y11}\cos\delta_{11} + F_{y12}\cos\delta_{12})r_{t1} + M_{T1}$$

$$m_{A2}\ddot{z}_{A2} - m_{A2}(\dot{x}_{A2}\dot{\theta}_{A2} - \dot{y}_{A2}\dot{\phi}_{A2}) = (F_{CL21} + F_{CL22}) - (F_{AirK21} + F_{AirK22}) + m_{A2}g(1 - \cos\theta_{A2}\sin\phi_{A2})$$

$$m_{A2}\ddot{y}_{A2} - m_{A2}(\dot{z}_{A2}\dot{\phi}_{A2} - \dot{x}_{A2}\dot{\psi}_{A2}) = F_{y21} + F_{y22} - F_{R2}^{'} - m_{A2}g\cos\theta_{A2}\sin\phi_{A2}$$

$$J_{xA2}\ddot{\phi}_{A2} - (J_{yA2} - J_{zA2})\dot{\psi}_{A2}\dot{\theta}_{A2} = (F_{CL21} - F_{CL22})b_2 + (F_{AirK22} - F_{AirK21})w_2 + F_{R2}(h_{R2} - r_{t2}) \\ +(F_{y21} + F_{y22})r_{t2} + M_{T2}$$

(2.3)

2.2. Hybrid Suspension System Model

The primary distinction of the proposed model lies in its hybrid suspension configuration. Specifically, the front axle utilizes mechanical spring-damper elements, whereas the rear axle employs pneumatic air springs. This structural asymmetry alters the roll stiffness distribution between the two axles, which consequently affects the vertical load transfer during cornering maneuvers. In this study, this mechanism serves as the fundamental basis for explaining how the hybrid suspension influences the tire friction saturation process and the lateral stability limits. The suspension forces at the front axle are described using a linear spring-damper model, formulated as follows:

$$\begin{cases} F_{C1j} = \begin{cases} C_{\infty}(z_{A1j} - z_{1j} + f_{dij}^{n}) & when\, f_{dij}^{n} < z_{A1j} - z_{1j} \\ C_{1j}(z_{A1j} - z_{1j}) & when\, f_{dij}^{t} \le z_{A1j} - z_{1j} \le f_{d1j}^{n} \\ -C_{\infty}(z_{A1j} - z_{1j} - f_{dij}^{n}) & when\, z_{A1j} - z_{1j} < f_{d1j}^{n} \end{cases} \\ F_{K1j} = K_{1j}(\dot{z}_{A1j} - \dot{z}_{1j}) \end{cases}$$

(2.4)

Where C_{1j} and K_{1j} denote the stiffness and damping coefficients of the front suspension, respectively; z_{1j} is the vertical displacement of the vehicle body at the suspension mounting point; and z_{A1j} represents the vertical displacement of the front axle at the corresponding location.For the rear axle, the suspension force comprises the pneumatic elastic force and the equivalent damping force, formulated as follows:

$$F_{AirK2j} = \begin{cases} F_{Air2j} = (P_{2j} - P_a)A_e + Ce_{2j}(z_{A2j} - z_{2j}) + Cv_{2j}(z_{A2j} - z_{2j} - w_{s2j}) \\ F_{K2j} = K_{2j}(\dot{z}_{A2j} - \dot{z}_{2j}) \end{cases} \quad (j = 1 \div 2)$$

(2.5)

Where: F_{Air2j} represents the force generated by the pneumatic air spring, and F_{K2j} is the
(2.3)
equivalent damping force of the rear suspension system. According to the GENSYS modeling approach, the dynamic characteristics of the air spring are governed by the internal air pressure, effective area, chamber volume, suspension deflection, and the parameters of the connecting pipe and auxiliary reservoir if equipped. Furthermore, previous studies on air suspension systems have demonstrated that the operating pressure, auxiliary reservoir volume, alongside the length and cross-sectional area of the connecting pipe, significantly influence the dynamic stiffness

and overall motion stability of the vehicle.The dynamic equation governing the air flow within the connecting pipe is expressed as follows:

$$M_{2j}\ddot{w}_{s2j} = C_{v21}(z_{2j} - w_{s2j}) - K_{m2j}\left|\dot{w}_{s2j}\right|^{\varepsilon} sign(\dot{w}_{s2j})$$
$$\varepsilon = 2; j = 1 \div 2$$

(2.6)

The static load depends on the amount of gas in the gas spring as follows:

$$F_{zt2j} = (P_{2j} - P_a)A_e \tag{2.7}$$

Where P_{2j} denotes the initial pressure; P_a is the atmospheric pressure; A_e represents the effective area of the air spring; M_{2j} is the mass of the air within the connecting pipe; w_{s2j} denotes the displacement of the air mass inside the pipe.

2.3. Wheel Dynamics

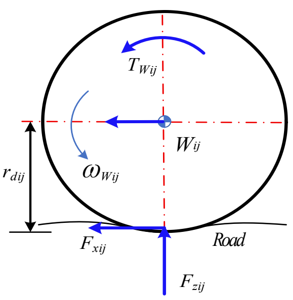

Figure.2. Schematic dynamics of the wheels [15]

The rotational dynamics of the wheels are analyzed to determine the longitudinal slip and the corresponding longitudinal tire forces. For the ij wheel, the equation of rotational motion is expressed as follows**:**

$$J_{Wij}\dot{\omega}_{Wij} = T_{ij} - F_{xij}rd_{ij} \quad (i = 1 \div 2; j = 1 \div 2)$$

(2.8)

Where J_{Wij} denotes the moment of inertia of the wheel; $\dot{\omega}_{Wij}$ is the wheel angular velocity; T_{ij} represents the driving torque applied to the wheel; F_{xij} is the longitudinal tire force; and rd_{ij} denotes the effective rolling radius of the wheel.

For the investigated 1.25-ton truck, the front wheels serve as the steered wheels. The steering angle of the left front wheel is determined directly from the steering wheel input as follows:

$$\begin{cases} \delta_{11} = \dfrac{\delta_w}{i_{sw}} \\ \cot\delta_{12} - \cot\delta_{11} = \dfrac{b_1}{2L} \end{cases} \tag{2.9}$$

Where δ_w denotes the steering wheel angle, and i_{sw} = 19:1 is the steering gear ratio. Subsequently, the steering angle of the right front wheel is determined based on the Ackermann steering geometry, which b_1 is the front track width, and L represents the wheelbase of the vehicle.

2.4. Burckhardt Tire Model

The Burckhardt tire model is employed to determine the tire-road interaction forces. This model is highly suitable for investigating lateral stability, as it can accurately capture the variation of the friction coefficient as a function of the resultant slip under various road conditions. In existing literature on commercial trucks and articulated vehicles, the Burckhardt model is frequently integrated with spatial multibody dynamics to analyze lateral instability mechanisms.

The resultant friction coefficient is formulated as follows:

$$\mu(s) = C_1(1 - e^{-C_2 s}) - C_3 s) \tag{2.10}$$

Where s denotes the resultant slip; C_1, C_2 ,and C_3 represent the empirical coefficients that depend on the specific road surface conditions. In this study, three representative road types are selected for the simulation scenarios. The specific coefficients for the Burckhardt model corresponding to these surfaces are detailed in Table 1.

Table 1. Empirical coefficients of the Burckhardt model

Road surface type	**C_1**	**C_2**	**C_3**	**Note**
Dry asphalt road	1.281	23.99	0.52	High friction coefficient
Wet gravel road	0.4004	33.7080	0.1204	Low friction coefficient
Ice-covered road	0.05	306.39	0.00	Very low friction coefficient

Under combined slip conditions, the resultant slip is determined as follows:

$$s = \sqrt{s_x^2 + s_y^2} \tag{2.11}$$

The longitudinal and lateral tire forces at the ij wheel are calculated using the following equations:

$$F_{xij} = \frac{s_{xij}}{\sqrt{s_{xij}^2 + s_{yij}^2}} \left(C_1 \left(1 - e^{-C_2\sqrt{s_{xij}^2 + s_{yij}^2}} \right) - C_3 \sqrt{s_{xij}^2 + s_{yij}^2} \right) F_{zij}$$

$$F_{yij} = \frac{s_{yij}}{\sqrt{s_{xij}^2 + s_{yij}^2}} \left(C_1 \left(1 - e^{-C_2\sqrt{s_{xij}^2 + s_{yij}^2}} \right) - C_3 \sqrt{s_{xij}^2 + s_{yij}^2} \right) F_{zij}$$

(2.12)

Where F_z denotes the vertical load acting on the wheel; s_x and s_y represent the longitudinal and lateral slip ratios, respectively.

The longitudinal slip ratio is formulated as:

$$s_{xij} = \begin{cases} -\dfrac{\dot{x}_{ij} - rd_{ij}.\omega_{W\,ij}}{\dot{x}_{ij}} & when\ -1 \le s_{xij} \le 0 \\ \dfrac{rd_{ij}.\omega_{W\,ij} - \dot{x}_{ij}}{rd_{ij}.\omega_{Wij}} & when\ 0 \le s_{xij} \le 1 \end{cases}$$

(2.13)

Where $\dot{x}_{ij}$ is the longitudinal velocity at the wheel center.For the steered wheels, the lateral slip ratio is determined based on the lateral velocity at the wheel center and the steering angle: $s_{yij} = \delta_{1j} - a\tan\left(\dfrac{\dot{y}_C + l_i \dot{\psi}_C}{\dot{x}_{ij} \pm 0.5 b_i \dot{\psi}_C} \right)$

(2.14)

For the non-steered wheels on the rear axle, $\delta_{2j} = 0$

2.5. Evaluation Criteria for Lateral Stability

To evaluate the lateral stability limits of the investigated 1.25-ton commercial truck featuring a hybrid suspension system, this study employs three primary indices: lateral acceleration, Load Transfer Ratio (LTR), and the tire friction utilization coefficient.

$$a_y = \dot{v}_y + v_x r \tag{2.15}$$

These indicators were selected as they directly capture the two fundamental instability mechanisms of the vehicle: rollover induced by dynamic load transfer and sideslip resulting from tire friction saturation.

In existing literature concerning truck lateral stability, parameters such as the LTR, lateral acceleration, roll angle, and tire friction-related indices are frequently utilized to define rollover thresholds, early warning boundaries, and critical instability states during cornering or emergency evasive maneuvers [5,10,16,17].The lateral acceleration of the vehicle body is calculated as follows:

Where v_x and v_y denote the longitudinal and lateral velocities of the vehicle body, respectively; and r is the yaw rate around the vertical axis. Physically, the lateral acceleration is constrained by the tire-road friction limit: $a_y \le \mu g$

However, to provide an early assessment of critical states, this study adopts a safety threshold: $a_{y,\lim} = 0.5\mu g$ .When $a_y > a_{y,\lim}$ the lateral acceleration exceeds this threshold, the vehicle is considered to be entering a hazardous lateral stability zone.

Furthermore, the rollover risk is evaluated using the LTR at each axle:

$$LTR_i = \frac{F_{zi2} - F_{zi1}}{F_{zi2} + F_{zi1}} \quad (i = 1 \div 2) \qquad (2.16)$$

Where F_{zi2} and F_{zi1} represent the vertical loads acting on the left and right wheels of the (i) axle, respectively. When LTR = 1, the vertical load on one wheel of that axle reaches zero, corresponding to a wheel lift-off condition. In this study, LTR=0.8 is adopted as an early warning threshold for rollover tendency, whereas LTR=1.0 is used as the wheel lift-off criterion. Therefore, values of LTR greater than 0.8 indicate a hazardous load transfer state, while LTR=1.0 represents a critical rollover condition[5,10].The risk of side-slip is assessed via the tire friction utilization coefficient:

$$\eta_{ij} = \frac{\sqrt{F_{xij}^2 + F_{yij}^2}}{\mu_{peak} F_{zij}}$$
$$\eta_{\max} = \max(\eta_{11}, \eta_{12}, \eta_{21}, \eta_{22})$$

(2.17)

Where F_x, F_y, and F_z are the longitudinal force, lateral force, and vertical load at the corresponding wheel, respectively. The parameter μ_{peak} is the maximum value of the Burckhardt friction curve for a given road surface. When $\eta_{max} \approx 1$, the resultant tire force approaches the available adhesion limit, indicating a high risk of directional side-slip [7,13,14].

3. Simulation Results and Evaluation

The simulation model is developed for a 1.25-ton commercial truck equipped with a hybrid suspension system. Fundamental geometric and mass parameters, including the wheelbase, track width, and gross vehicle weight, are adopted directly from the technical specifications of a typical 1.25-ton light commercial truck. Parameters not provided in the manufacturer's catalog, such as the center of gravity CG height and mass moments of inertia, are determined through geometric estimation methods based on the vehicle's mass distribution. The digital techniques are presented in Table 2.

Table 2**.** Basic parameters of the investigated truck

Specifications	Value
Vehicle's total load	2985 kg
Gravitational acceleration	9.81 m/s^2
Wheelbase	2.585 m
Front wheel track width	1.490 m
Moment of inertia around the x-axis of the vehicle body. (J_{xC})	1513 kg.m^2
Moment of inertia around the z-axis of the vehicle body. (J_{zC})	6335 kg.m^2
Moment of inertia around the y-axis of the vehicle body. (J_{yC})	6514 kg.m^2
Effective area of a pneumatic spring A_e	0.025m^2
Initial pressure of the pneumatic spring (P_{2j})	4.5x10^5 Pa
Front axle suspension stiffness (C_{1j})	86920 N/m
Front axle damping coefficient (K_{1j})	9692 Ns/m

Simulations were conducted to evaluate the effects of vehicle speed and road adhesion on the lateral stability of the 1.25-ton truck during a J-turn maneuver. The hybrid suspension configuration was kept unchanged in all simulation cases. First, the vehicle speed was varied from 30 to 60 km/h on dry asphalt to investigate the speed-dependent rollover tendency. Then, three road adhesion conditions, including dry asphalt, wet gravel, and ice-covered roads, were considered at a fixed speed of 50 km/h to identify the transition between rollover and side-slip mechanisms. Finally, a rollover–side-slip stability boundary map was constructed by combining vehicle speed and road adhesion conditions.The J-turn maneuver was

$$\delta_w(t) \begin{cases} 0, & t < t_0 \\ \delta_{w0}\left(1 - e^{\frac{t-t_0}{\tau}}\right) & t \geq t_0 \end{cases} \qquad (2.18)$$

employed to simultaneously excite the lateral and roll dynamics. To avoid unrealistic abrupt steering inputs, the steering angle smoothly increases to a predefined steady-state value, formulated as:

Where δ_w is the steering wheel angle; δ_{w0} is the target angle; t_0 is the steering start time; and τ is the time constant governing the steering rate.The dynamic response is evaluated using lateral acceleration a_y, roll angle ϕ, LTR, and tire friction utilization η. By monitoring these indices, the primary instability mechanism is distinguished: if the LTR threshold is exceeded first, the vehicle is prone to rollover; conversely, if the η reaches its limit first, directional side-slip dominates.

3.1. Effect of Vehicle Speed on Lateral Response

In this investigation, the vehicle is simulated on a dry asphalt surface with a steering wheel input of 120°. The evaluated speeds are 30, 40, 50, and 60 km/h. The lateral acceleration early-warning threshold is established at 0.5 μg = 5.74 m/s², whereas the theoretical adhesion limit of the road surface is μg = 11.49 m/s². Furthermore, the rollover warning threshold is set at LTR = 0.8, while the critical wheel lift-off condition occurs at LTR = 1.

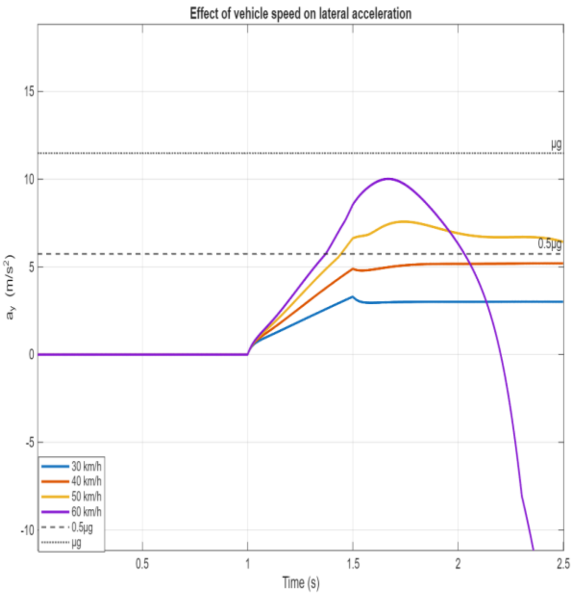

Figure3. Effect of vehicle speed on lateral acceleration.

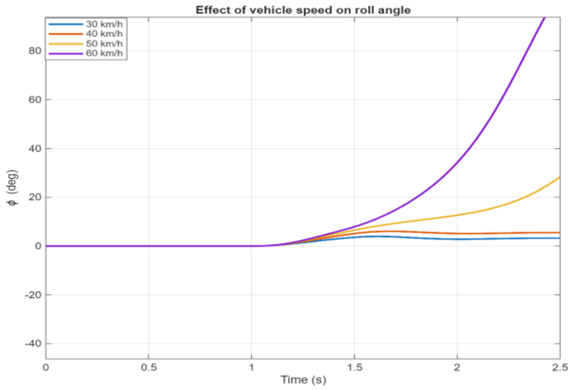

Figure. 4. Effect of vehicle speed on roll angle

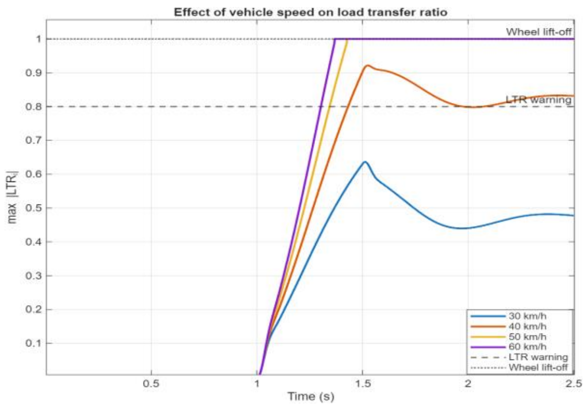

Figure. 5. Effect of vehicle speed on load transfer ratio

As illustrated in Figs. 3 and 4, the vehicle's maximum lateral acceleration a_{ymax} and roll angle φ_{max} increase significantly with speed. At 30 and 40 km/h, the dynamic responses remain moderate. However, at 50 km/h, a_{ymax} = 7.58 m/s² exceeding the 0.5μg early-warning threshold), and φ_{max} spikes to 28.34°. At 60 km/h, a_{ymax} surpasses the theoretical adhesion limit μg = 11.49 m/s², accompanied by an extreme simulated roll angle (>80°), indicating a complete loss of stability and a transition into the post-limit hazardous zone. Fig. 5 demonstrates that the LTR is the primary indicator of rollover risk. While stable at 30 km/h, the vehicle exhibits a clear rollover tendency at 40 km/h ,LTR_{max} = 0.922, exceeding the 0.8 warning threshold. At 50 and 60 km/h, LTR_{max} = 1.0, confirming critical wheel lift-off.

Higher speeds notably accelerate the onset of this instability.Crucially, the tire friction utilization coefficient η_{max} increases from 0.445 at 30 km/h to approximately 1.0 at 60 km/h. At 40 and 50 km/h, the LTR reaches its critical threshold before η_{max} achieves saturation. This confirms that rollover induced by dynamic load transfer is the dominant instability mechanism for this hybrid suspension truck on dry asphalt. A combined failure mode of rollover and tire saturation is only observed at extreme speeds 60 km/h.In conclusion, vehicle speed fundamentally dictates lateral stability during cornering. For the investigated configuration, 40 km/h serves as the early-warning boundary, whereas speeds of 50 km/h and above constitute a critical rollover hazard zone.

3.2. Influence of Road Adhesion on Vehicle Lateral Stability

The simulation results illustrating the impact of road adhesion conditions are presented in Figs. 6-8. For this analysis, the vehicle is evaluated at a constant speed of 50 km/h with a consistent steering wheel input across three distinct road surfaces: dry asphalt, wet gravel and ice. The tire friction characteristics are defined using the Burckhardt model. The stability assessment relies on previously established thresholds: 0.5μg for the lateral acceleration early warning, μg for the theoretical adhesion limit, LTR = 0.8 for the rollover warning, and LTR = 1 for the critical wheel lift-off condition.As shown in Fig. 6, the maximum lateral acceleration is strongly affected by road adhesion. On dry asphalt, a_{ymax} = 7.58 m/s², exceeding the early warning threshold. When the road adhesion decreases, the lateral acceleration decreases to 3.34 m/s² on wet gravel and 0.36 m/s² on ice. This confirms that low road adhesion limits the lateral force generation capability of the tires.Fig. 7 shows that rollover tendency is mainly observed on the high-adhesion road. On dry asphalt, the LTR of both axles approaches 1.0, indicating wheel lift-off. On wet gravel and ice, the LTR remains below the warning threshold of 0.8, suggesting that rollover is not the dominant instability mechanism under these low-adhesion conditions.The hybrid suspension configuration also produces an uneven load transfer distribution between the front and rear axles.

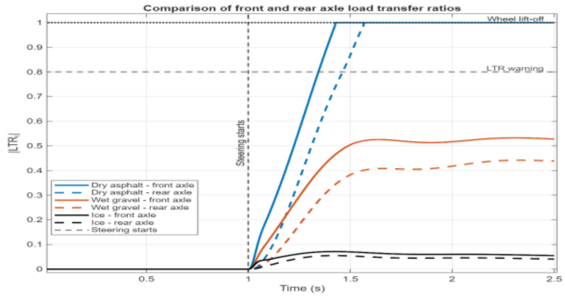

Figure.6. Effect of road adhesion on lateral Acceleration

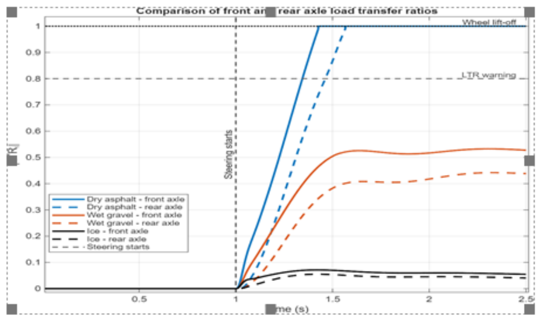

Figure.7.Comparison of front and rear axle load transfer ratios

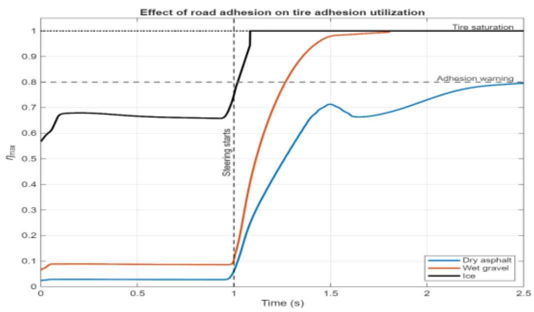

Figure.8. Maximum combined tire adhesion utilization

Under non-saturated LTR conditions, the front axle consistently exhibits a higher LTR than the rear axle, as shown in Table 3. On wet gravel, $LTR_{front,max}$= 0.533, whereas $LTR_{rear,max}$= 0.442, corresponding to a 17.01% relative difference. On ice, the corresponding values are 0.071 and 0.055, respectively. This trend indicates that the front mechanical suspension responds more strongly to lateral load transfer, while the rear pneumatic suspension tends to soften the rear axle load transfer response. However, this conclusion is limited to the present model because no conventional suspension reference model is included for direct comparison.

Table 3. Uneven load transfer distribution between the front and rear axles.

Road Condition	$LTR_{front, max}$	$LTR_{rear, max}$	Distribution difference	Relative Difference (Front > Rear)
Dry asphalt	1.00	1.00	0.00%	0.00%
Wet gravel	0.533	0.442	9.30%	17.01%
Ice	0.071	0.055	12.84%	22.77%

(Note: Values plateau at 1.0 due to physical wheel lift-off).

According to Fig. 8, the maximum combined tire friction utilization reaches saturation earlier on low-adhesion roads. On dry asphalt, η_{max} = 0.797, indicating that the tire forces remain below the adhesion limit. In contrast, η_{max} = 1.0 on wet gravel and ice while the LTR remains below the rollover warning threshold. Therefore, the dominant instability mechanism shifts from rollover on dry asphalt to side-slip on low-adhesion surfaces.

3.3. Rollover-sideslip stability boundary map

The rollover and side-slip stability boundary map is presented in Fig. 9. The map is constructed as a function of vehicle speed and road adhesion under a constant steering wheel input of 120°. The vehicle stability state is classified using two indices: the LTR and the maximum combined tire friction utilization η_{max}. In this study, LTR = 0.8 is used as the rollover warning threshold, LTR = 1.0 represents wheel lift-off, and η_{max} = 1.0 indicates tire friction saturation.

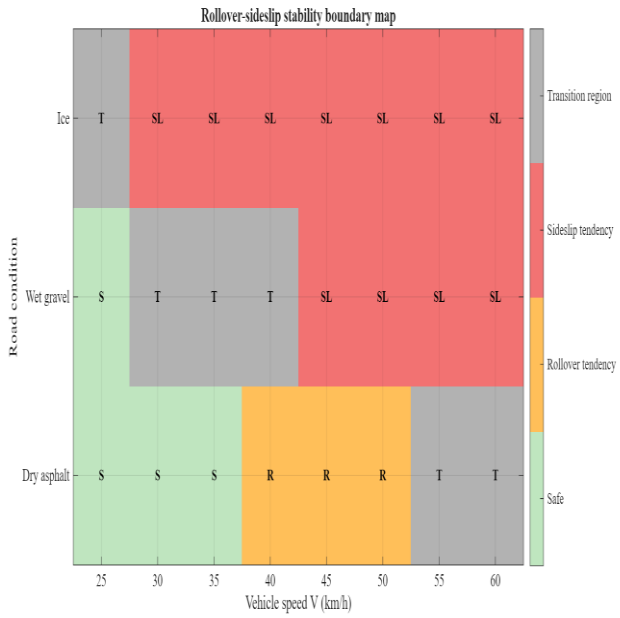

Figure.9. Rollover-sideslip stability boundary map

On dry asphalt, the vehicle remains stable from 25 to 35 km/h, where both LTR_{max} and η_{max} remain below the critical thresholds. At 40 km/h, LTR_{max} exceeds the 0.8 warning threshold, indicating the onset of rollover tendency. From 45 to 50 km/h, LTR_{max} reaches approximately 1.0, corresponding to wheel lift-off. At 55–60 km/h, both LTR_{max} and η_{max} approach unity, indicating a combined critical condition involving both rollover and tire friction saturation. On wet gravel, the safe region is limited to approximately 25 km/h. Between 30 and 40 km/h, the vehicle enters a transition region where η_{max} approaches the adhesion limit, while LTR_{max} remains below the rollover warning threshold. From 45 km/h upward, η_{max} = 1.0, whereas LTR_{max} remains below 0.8, indicating that side-slip becomes the dominant instability mechanism. On ice, the vehicle operates close to the tire adhesion limit throughout the investigated speed range. The value of η_{max} reaches approximately 1.0 even at low speed, whereas LTR_{max} remains very small. This indicates that the instability mechanism on ice is governed mainly by tire friction saturation rather than rollover.

Overall, the stability boundary map shows that the vehicle stability limit is jointly governed by speed and road adhesion. On high-adhesion roads, large lateral tire forces lead to significant load transfer through the suspension system and promote rollover. On low-adhesion roads, tire friction saturation occurs before the LTR reaches a critical level, and the dominant instability mechanism shifts toward side slip.

4. Conclusion

This study investigated the lateral stability limits of a 1.25-ton light commercial truck equipped with a hybrid suspension system consisting of a front mechanical suspension and a rear pneumatic suspension. A spatial multibody dynamic model was combined with the Burckhardt tire model to evaluate the effects of vehicle speed and road adhesion on rollover and side-slip tendencies during a J-turn maneuver. The stability response was assessed using lateral acceleration, roll angle, load transfer ratio, and maximum combined tire friction utilization. The simulation results show that vehicle speed strongly affects rollover stability on high-adhesion roads. On dry asphalt, the vehicle remains stable at 30 km/h, with aymax of 0.30 m/s² and LTRmax of 0.636. At 40 km/h, LTRmax increases to 0.922, exceeding the rollover warning threshold, whereas tire friction utilization remains below saturation. From 50 km/h, LTRmax reaches approximately 1.0, indicating wheel lift-off. At 60 km/h, aymax = 12.31 m/s² exceeds the theoretical adhesion limit, and ηmax approaches unity, indicating a combined critical state involving both rollover and tire friction saturation. The road adhesion condition changes the dominant instability mechanism. At 50 km/h, dry asphalt allows large lateral forces to develop, leading to severe load transfer and rollover tendency. In contrast, on wet gravel and ice, the LTR remains below the rollover warning threshold, while ηmax reaches unity. This indicates that, under low-adhesion conditions, the stability limit is governed mainly by tire friction saturation and directional side-slip rather than rollover. The hybrid suspension configuration affects the distribution of load transfer between the two axles. Under low-adhesion conditions, the front axle exhibits a higher LTR than the rear axle. The front axle LTR is 17.01% higher than the rear axle on wet gravel and 22.77% higher on ice. This suggests that the front mechanical suspension is more sensitive to lateral load transfer, whereas the rear pneumatic suspension provides a softer rear axle response. However, this interpretation is limited to the present numerical model, and a direct comparison with a conventional suspension configuration is required to quantify the stabilizing contribution of the rear air suspension. The stability boundary map confirms that the safe operating envelope depends on both vehicle speed and road adhesion. For the investigated J-turn maneuver, the vehicle remains within the safe region up to approximately 35 km/h on dry asphalt and 25 km/h on wet gravel. On ice, the vehicle operates close to the tire adhesion limit across the investigated speed range. These results provide a useful basis for defining rollover–side-slip warning thresholds and for developing stability control strategies for light commercial trucks equipped with hybrid suspension systems. Future work should include experimental validation and comparison with a conventional suspension model to further verify the proposed conclusions.

Acknowledgement

Authors are responsible for ensuring that all individuals named in this section have provided their consent to be acknowledged.

Funding

This study was not supported by any grants from funding bodies in the public, private, or not-for-profit sectors.

Declaration of Competing Interest

The author declares no conflicts of interest.

CRediT Authorship Contribution Statement

Authors are encouraged to provide a detailed statement outlining their specific roles and contributions to the manuscript, in accordance with the journal's authorship policy. The corresponding author is responsible for ensuring that all listed authors have reviewed and agreed upon the accuracy of their reported contributions.

- Conceptualization : Vu Duong, Nguyen Thanh Tung
- Methodology : Tung Nguyen Thanh,
- Software : Khoi Phan Chuong Anh

- Validation : Vu Duong, Khoi Phan Chuong Anh
- Formal analysis : Vu Duong, Khoi Phan Chuong Anh
- Investigation : Vu Duong, Khoi Phan Chuong Anh
- Data curation : Vu Duong, Khoi Phan Chuong Anh
- Writing – original draft : Khoi Phan Chuong Anh
- Visualization : Vu Duong
- Supervision: Vu Duong

Generative Artificial Intelligence Declarations

The authors claim that artificially intelligent-assisted technologies,, such as generative AI, were not used to generate content, ideas, or theories.

References

[1] TA Tuan Hung, DUONG Ngoc Khanh, VO Van Huong," Study on Effects of Road Conditions on the Lateral Instability of Tractor Semitrailer Vehicle during Turning Maneuver". *Engineering and Technology for Sustainable Development,* 32(2**),** 074-080,2022. https://doi.org/10.51316/jst.157.etsd.2022.32.2.10.

[2] Chen, M., Zhou, L., Choo, S., Lee, H.,"Analysis of risk factors affecting urban truck traffic accident severity in Korea", *Sustainability* ,14(5), 2901,2022. doi:10.3390/su14052901

[3] Mustafa, A.E., Mümin, T.E., Basar, O.,"Lateral stability control of articulated heavy vehicles based on active steering system", *International Journal of Mechanical Engineering and Robotics Research,*11(8), 575–582,2022. doi:10.18178/ijmerr.11.8.575-582

[4] Ta, T.H., Duong, N.K.,"Analysis the dynamic rollover threshold and roll safety thresholds of 4-axle truck vehicle: a simulation approach", International Journal on Interactive Design and Manufacturing,2024. doi:10.1007/s12008-024-02117-1

[5] Lundahl, K., Berntorp, K., Olofsson, B., Nielsen, L.,"Analyzing rollover indices for critical truck maneuvers", SAE International Journal of Commercial Vehicles ,8(1), 194–205,2015. doi:10.4271/2015-01-1595

[6] Guan, H., Chen, B., Zhang, X., Wu, J.," Rollover stability analysis of heavy vehicles based on load transfer ratio", Chinese Journal of Mechanical Engineering ,27, 965–971,2014 . doi:10.3901/CJME.2014.0725.128

[7] Yanna, Y., Huiying, W., Lu, S., Wei, H.," Study on the influence of road geometry on vehicle lateral instability", *Journal of Advanced Transportation* , 1–15,2020.

[8] Rajamani, R.Vehicle Dynamics and Control, 2nd edn. Springer, New York,2012

[9] Jazar, R.N.*Vehicle Dynamics: Theory and Application*, 3rd edn. Springer, Cham,2017

[10] Mitschke, M., Wallentowitz, H.," Dynamik der Kraftfahrzeuge, 4th edn,2004.

[11] Cebon, D.Handbook of Vehicle-Road Springer, Berlin .Interaction. Swets & Zeitlinger, Lisse,1999 .

[12] Soltani, A., Assadian, F.,"New vehicle rollover prevention system based on active steering and differential braking", SAE Technical Paper, 2015-01-0656,2015 . doi:10.4271/2015-01-0656

[13] Dong, G., Chen, S., Wu, J., Zhang, Y.,"Rollover warning and prevention for heavy vehicles based on lateral load transfer ratio", Advances in Mechanical Engineering, 10(7), 1–13,2018 . doi:10.1177/1687814018789505

[14] Tung Nguyen Thanh,Luong Van Van.," A study on the vibration of a bus with air suspension system moving on random road surface profiles with different speeds", Engineering Solid Mechanics ,11(2):119-124,2023. DOI: 10.5267/j.esm.2023.1.004

[15] Ta, T.H., Duong, N.K.,"Simulation approach to investigate the influence of the steering wheel angle and vehicle speed on the rollover of a 4-axle truck vehicle during turning maneuvers", JST: Smart Systems and Devices, 35(1),065–

073,2025. doi:10.51316/jst.179.ssad.2025.35.1.8

[16] Burckhardt,M.Fahrwerktechnik: Radschlupf-Regelsysteme.Vogel-Verlag, Würzburg,1993 .

[17] Tran, V.N., Nguyen, X.N., Vu, V.T., Dang, T.P.,"Rollover stability analysis of liquid tank truck taking into account the road profiles", Journal of Applied Engineering Science, 20(4), 1133–1142,2022. doi:10.5937/jaes0-36578